CHEMISTRY OF MATERIALS

Article

Hg-Based Infrared Nonlinear Optical Material KHg4Ga5Se12 Exhibits Good Phase-Matchability and Exceptional Second Harmonic Generation Response

Molin Zhou, Yi Yang, Yangwu Guo, Zheshuai Lin, Jiyong Yao, Yicheng Wu, and Chuangtian Chen

Chem. Mater., **Just Accepted Manuscript** • DOI: 10.1021/acs.chemmater.7b03143 • Publication Date (Web): 29 Aug 2017

ACS Publications

Chemistry of Materials is published by the American Chemical Society. 1155 Sixteenth Street N.W., Washington, DC 20036

Hg-Based Infrared Nonlinear Optical Material $KHg_4Ga_5Se_{12}$ Exhibits Good Phase-Matchability and Exceptional Second Harmonic Generation Response

Molin Zhou,[†,‡] Yi Yang,[†,‡] Yangwu Guo,[†,‡] Zheshuai Lin,[†] Jiyong Yao,[*,†] Yicheng Wu[†] Chuangtian Chen[†]

[†] Beijing Center for Crystal Research and Development, Key Laboratory of Functional Crystals and Laser Technology, Technical Institute of Physics and Chemistry, Chinese Academy of Sciences, Beijing 100190, P.R. China

[‡] University of Chinese Academy of Sciences, Beijing 100049, P.R. China

[*]Corresponding author: Jiyong Yao; jyao@mail.ipc.ac.cn

ABSTRACT

High-performance infrared (IR) nonlinear optical (NLO) materials with large NLO response and suitable birefringence are urgently needed for various applications. A Hg-based IR NLO material $KHg_4Ga_5Se_{12}$ with such desirable properties has been newly discovered. In the structure, obviously distorted $HgSe_4$ and $GaSe_4$ tetrahedra are connected to each other by vertex-sharing to form a three-dimensional framework with the counter-ion K^+ residing in the cavities. Remarkably, all the NLO-active building units in the title compound are arranged in a completely parallel manner. Such a topological structure and the large susceptibility of the Hg−Se bonds enable the material to achieve good phase-matchability with a tremendous powder SHG response at 2.09 μm that is about 20 times that of the benchmark material $AgGaS_2$ (one of the largest responses among all the phase-matchable IR NLO chalcogenides reported to date). The optical band gap of $KHg_4Ga_5Se_{12}$ was determined as 1.61 eV. Moreover, based on the electronic band structure, the real-space atom-cutting analysis, the SHG-weighted electronic densities, and the local dipole moments calculations, the origin of the superior linear and nonlinear optical properties of the title compound is ascribed to the $(Hg/Ga)Se_4$ group. The calculated values for the maximum coefficient d_{33} and birefringence (Δn) at 2.09 μm are −65.257 pm/V and 0.072, respectively. Such values agrees well with experimental observations. Our study demonstrates that Hg-based metal chalcogenides are a class of IR NLO material with competitive features (good phase-matchability, very large SHG efficiency, wide transparency) desirable for practical applications.

INTRODUCTION

The growing demands for new IR coherent light sources have stimulated large-scale tentative synthetic activities in searching new IR NLO crystals, which can convert the frequencies of existing lasers to a favorable wavelength range with reasonable efficiency by second harmonic generation (SHG), sum frequency generation (SFG), difference frequency generation (DFG), optical parametric amplification (OPA) and optical parametric oscillation (OPO) processes, etc.[1-6] The chalcopyrite-type ternary compounds $AgGaQ_2$ (Q = S, Se)[7,8] and $ZnGeP_2$[9] are known as the benchmark IR NLO materials for decades. Unfortunately, all of them are subject to property shortcomings that severely restrict their further applications. Therefore, searching for alternatives with good overall performances are of significant importance.

As a rich family of compounds, metal chalcogenides, offer a fruitful source of potential IR NLO materials owing to their wide compositional and structural flexibility and inherently good optical transparency in the mid- and far-IR regions. By applying various synthetic strategies, many interesting IR NLO crystals have been successfully synthesized in the past several years. Some representing examples include $LiMQ_2$ (M = Ga, In; Q = S, Se),[10-12] $AAsSe_2$ (A = Li, Na),[13] $BaGa_4Q_7$ (Q = S, Se),[14,15] $SnGa_4Q_7$ (Q = S, Se),[16] Na_2BaMQ_4 (M = Ge, Sn; Q = S, Se),[17] $Ba_{23}Ga_8Sb_2S_{38}$,[18] and $Ba_2Ga_8MS_{16}$ (M = Si, Ge),[19] etc.

Very recently, our interests in the search for new IR NLO crystals have mainly focused on the d^{10} cations-containing metal chalcogenides, especially the Hg-based

ones, owing to the following thoughts: (1) Hg^{2+} is about the same size as Ca^{2+}, but it is a much more strongly polarizing ion as a result of the decreased shielding power of the 4*f* electrons and relativistic effects. Thus, the ion has a strong tendency to form covalent bonds rather than ionic bonds, especially with S-, Se-ligands and the Hg−chalcogens bonds should exhibit wide transparent window in the IR region. (2) The outer electron configuration of mercury is $6s^2$, the closed-shell configuration can effectively avoid the *d*-*d* optical transition problem. Moreover, the outer orbital energies are very close and little energy is required to promote an electron from the 6*s* orbital to one of the 6*p* orbitals. In this case, the orbitals can combine to form sp^x hybrid orbitals to form linear, trigonal-planar, and tetrahedral coordination for x = 1, 2, and 3 respectively. The trigonal-planar units and the tetrahedral units are typical NLO-active structural units. In addition, the highly polarizable Hg-chalcogen bond would further increase the SHG response and the birefringence of IR NLO materials. Hence, Hg-based chalcogenides may provide an attractive playground for IR-NLO materials (it should be mentioned that element Hg and most of the Hg-based compounds are extremely toxic and unfriendly to the environment. Therefore, all the manipulations should be performed with great care). According to our investigation, only a few Hg-based metal chalcogenides have been reported as promising IR NLO materials including $HgGa_2S_4$,[20] $BaHgQ_2$ (Q = S, Se),[21,22] Li_2HgMS_4 (M = Si, Ge, Sn),[23] $Li_4HgGe_2S_7$,[24] and $A_2Hg_3M_2S_8$ (A = Na, K; M = Si, Ge, Sn).[25,26] In particular, the $[HgSe_3]^{4-}$ groups in $BaHgSe_2$ were identified as the first π-conjugated anionic groups with large NLO susceptibilities and stable chemical properties in IR NLO

materials.[22] Among these Hg-based IR NLO materials, the largest SHG response was reported to be 6.5 times that of $AgGaS_2$.

As part of our recent explorations for promising Hg-based IR NLO materials, we report in this paper a new Hg-based compound $KHg_4Ga_5Se_{12}$, which features a three-dimensional framework composed of vertex-sharing $HgSe_4$ and $GaSe_4$ tetrahedra with the counter-ion K^+ residing in the cavities. Interestingly, all of the NLO-active chromophores ($HgSe_4$ and $GaSe_4$ tetrahedra) in $KHg_4Ga_5Se_{12}$ are arranged in a completely parallel manner. Owing to such a cooperative packing mode and the highly susceptible Hg−Se bonds, the material displays good phase-matchability with a tremendous powder SHG responses at 2.09 μm that is about 20 times that of the benchmark material $AgGaS_2$. Such intense NLO response is one of the largest among all phase-matchable IR NLO materials reported so far. This work demonstrates that Hg-based metal chalcogenides may be promising alternatives for IR nonlinear optics, and may provide some insights in the further search for new IR NLO materials. Herein, we represent the synthesis, crystal structure, linear and nonlinear optical properties and the detailed theoretical calculations of this new IR NLO material.

EXPERIMENTAL SECTION

Synthesis. K (3N), Ga (5N), Se (5N) and HgSe (4N) were directly purchased from Sinopharm Chemical Reagent Co., Ltd. The binary starting materials K_2Se and Ga_2Se_3 were synthesized by the stoichiometric reaction of the elements in sealed silica tubes. All manipulations were performed in an Ar-filled glovebox with H_2O and O_2

contents less than 0.1 ppm. Polycrystalline sample of $KHg_4Ga_5Se_{12}$ was obtained by traditional solid state reaction[27-29] in a stoichiometric mixture of K_2Se, HgSe and Ga_2Se_3. The raw materials were loaded into fused-silica tubes and then, the ampoules were flame-sealed under a high vacuum of 10^{-3} Pa. The tubes were then placed in a computer-controlled furnace and heated to 873 K within 15 h, left for 48 h and, finally, the furnace was turned off.

Crystal Growth. Single crystals of $KHg_4Ga_5Se_{12}$ were prepared through spontaneous crystallization using excess K_2Se as flux. The reaction charge of K_2Se, HgSe and Ga_2Se_3 in a molar ratio of 3: 8: 5 was mixed and loaded into a fused-silica tube. Then, the tube was flame-sealed and gradually heated to 1123 K in a computer-controlled horizontal furnace, kept for 72 h, and then, slowly cooled at a rate of 3 K/h, and finally cooled to room temperature by switching off the furnace. The product consists of hundreds of dark-red block-shaped crystals. These small crystals were stable in air for more than 5 months by now. The EDX-equipped field emission scanning electron microscope (Hitachi S-4800) analysis on several small crystals confirmed the presence of K, Hg, Ga and Se in the molar ratio of approximately 1 : 4 : 5 : 12. Then a crystal with good morphology was manually selected for structure characterization.

Structure Determination. Single-crystal X-ray diffraction experiment was performed on a Xcalibur Ecos diffractometer equipped with a graphite-monochromated Mo-K_α (λ = 0.71073 Å) radiation at 293 K. The collection of the intensity data and cell refinement was carried out with CrysAlisPro software

(Agilent Technologies, Version 1.171.35.11).[30] Multi-scan absorption corrections were performed numerically with the use of the program XPREP.[31]

The structure was solved with the direct methods using SHELXTLS program and refined with the least-squares program SHELXL of the SHELXTL.PC program suite.[31] The main structural data and refinement parameters for $KHg_4Ga_5Se_{12}$ are given in Table 1. The atom positional coordinates and equivalent isotropic displacement parameters for the title compound are given in Table 2. The selected bond distances can be observed in Table 3.

Powder X-ray Diffraction (PXRD). The PXRD pattern of the ground powder was performed at room temperature on a Bruker D8 Focus diffractometer with Cu K_α (λ = 1.5418 Å) radiation. The scanning step width of 0.05º and a fixed counting time 0.2 s/step were applied to record the patterns in the 2θ range of 10 – 80º. The measured XRD powder pattern was found to perfectly match with the simulated pattern generated using the CIF of the refined structure. (see Figure 1).

Raman Spectroscopy. The unpolarized Raman scattering spectrum was recorded from ground powder sample at room temperature with an inVia-Reflex instrument with a line of 532 nm of solid state laser. The spectral resolution was 2 cm^{-1}, and the scanning range was 100 – 500 cm^{-1}.

Diffuse Reflectance Spectroscopy. Appropriate amount of $KHg_4Ga_5Se_{12}$ polycrystalline sample was thoroughly ground. A Cary 5000 UV-vis-NIR spectrophotometer with a diffuse reflectance accessory (the spectral resolution in the UV-vis and NIR range is 0.05 nm and 0.2 nm, respectively) was used to measure the

spectrum of the title compound and $BaSO_4$ (as a reference) in the range from 400 nm (3.1 eV) to 2000 nm (0.62 eV).

Thermal Analysis. By applying the Labsys™ TG-DTA16 (SETARAM) thermal analyzer equipped with the nitrogen flow at a rate of about 30 ml/min, the thermal stability of the title material was investigated in detail. Appropriate amounts of polycrystalline powder of $KHg_4Ga_5Se_{12}$ were thoroughly ground, then were placed in a silica tube (5 mm o.d. × 3 mm i.d.) and subsequently sealed under a high vacuum. The tube was heated from room temperature to 1273 K and then cooled to room temperature with the heating/cooling rate both at 15 K min^{-1}.

SHG Measurement. The optical SHG response of $KHg_4Ga_5Se_{12}$ was measured on polycrystalline powder samples by means of the Kurtz–Perry method.[32] The fundamental light was a 2090 nm light generated with a Q-switched Ho: Tm: Cr: YAG laser. The sample was thoroughly ground and sieved into a series of distinct particle size ranges of 20 − 41, 41 − 74, 74 − 105, 105 − 150 and 150 − 200 μm, respectively, which were then pressed into a disk with diameter of 8 mm that was put between glass microscope slides and secured with tape in a 1 mm thick aluminum holder. Microcrystalline $AgGaS_2$ was ground and sieved into the same particle size range of 150 − 200 μm as a reference.

COMPUTATIONAL SECTION

First-principles Calculation. The first-principles calculations for $KHg_4Ga_5Se_{12}$ were performed by CASTEP,[33] a plane-wave pseudopotential total energy package

based on density functional theory (DFT).[34] The functional developed by Perdew-Burke-Emzerhoff (PBE) functional within the generalized gradient approximation (GGA)[35,36] form were adopted to describe the exchange-correlation energy. The optimized norm-conserving pseudopotentials[37] in the Kleinman-Bylander[38] form for all the elements are used to model the effective interaction between atom cores and valence electrons. And K $3s^2 3p^6 4s^1$, Ga $3d^{10}4s^2 4p^1$, Hg $5s^2 5p^6 5d^{10} 6s^2$ and Se $4s^2 4p^4$ electrons were treated as valence electrons, allowing the adoption of a relatively small basis set without compromising the computational accuracy. The high kinetic energy cutoff 1000 eV and dense 2×2×4 Monkhorst-Pack[39] *k*-point meshes in the Brillouin zones were chosen for $KHg_4Ga_5Se_{12}$. For the calculations of the electronic structure, SHG coefficients and refractive indices, we used the structural data directly from the experimental determination, which means that we treated the disorder between Hg and Ga cations by the virtual crystal approximation (VCA) method rather than the super-cell method to conduct the first-principles simulations with a moderate computational cost. Our tests showed that the above computational setups are sufficiently accurate for present purposes.

Based on the scissor-corrected[40] electronic band structure, the imaginary part of the dielectric function was calculated according to the electron transition from the valence bands (VBs) to conduction bands (CBs). The real part of the dielectric function is obtained by the Kramers-Kronig[41] transform, from which the refractive indices are also determined. The second order susceptibility $\chi^{(2)}$ and the SHG

coefficients d_{ij} are calculated by the formula developed by our group.[42,43] The second-order susceptibility χ_{ijk} is represented as:

$$\chi_{ijk} = \chi_{ijk}(\mathrm{VE}) + \chi_{ijk}(\mathrm{VH}) + \chi_{ijk}(\mathrm{twobands})$$

where χ_{ijk} (VE) and χ_{ijk} (VH) denote the contributions from virtual-electron processes and virtual-hole processes, respectively, and χ_{ijk} (two bands) gives the contribution from two band processes to $\chi^{(2)}$. The formulas for calculating χ_{ijk} (VE), χ_{ijk} (VH) and χ_{ijk} (two bands) are as following:

$$\chi_{ijk}(\mathrm{VE}) = \frac{e^3}{2\hbar^2 m^3}\sum_{vcc'}\int\frac{d^3\vec{k}}{4\pi^3}\mathrm{P}(ijk)\,\mathrm{Im}[p^i_{vc}p^j_{cc'}p^k_{c'v}]\left(\frac{1}{\omega^3_{cv}\omega^2_{vc'}}+\frac{2}{\omega^4_{vc}\omega_{c'v}}\right)$$

$$\chi_{ijk}(\mathrm{VH}) = \frac{e^3}{2\hbar^2 m^3}\sum_{vv'c}\int\frac{d^3\vec{k}}{4\pi^3}\mathrm{P}(ijk)\,\mathrm{Im}[p^i_{vv'}p^j_{v'c}p^k_{cv}]\left(\frac{1}{\omega^3_{cv}\omega^2_{v'c}}+\frac{2}{\omega^4_{vc}\omega_{cv'}}\right)$$

$$\chi_{ijk}(\mathrm{twobands}) = \frac{e^3}{\hbar^2 m^3}\sum_{vc}\int\frac{d^3\vec{k}}{4\pi^3}\mathrm{P}(ijk)\frac{\mathrm{Im}[p^i_{vc}p^j_{cv}(p^k_{vv}-p^k_{cc})]}{\omega^5_{vc}}$$

Here, *i*, *j* and *k* are Cartesian components, *v* and *v'* denote VB, and *c* and *c'* denote CB. *P(ijk)* denotes full permutation. It should be emphasized that the refractive indices and SHG coefficients can be accurately obtained by DFT in principle because these optical properties are determined by the virtual electronic excited processes which are described by the first- and second-order perturbations, respectively, on the ground state wavefunctions.

RESULTS AND DISCUSSION

Structure. $KHg_4Ga_5Se_{12}$ belongs to an enormous compounds family in trigonal space group *R*3 with an overall formula $AM_4M'_5Q_{12}$,[44-47] where A, M, M' and Q represent an alkali metal cation with relatively large radius, a bivalent transition cation,

a trivalent main group cation and chalcogens, respectively. The most notable structural feature of the above family is a quasi-cubic closest packing of the chalcogen atoms with the tetrahedral interspaces occupied by M and M' cations. It is worth mentioning that lots of members in this family have been identified, in which the M and M' can accomodate various types of cations (Mn^{2+}, Zn^{2+}, Cd^{2+}, and Ga^{3+}, In^{3+}, *etc.* , respectively), showing rich substitutability of this structure model. However, our newly synthesized compound $KHg_4Ga_5Se_{12}$ is the first example in this family to place Hg^{2+} as the bivalent cation. We have also made a lot of attempts to synthesize other Hg-containing analogues, but unfortunately, the crystals of the In-containing selenide analogue were of poor quality in our synthesis and no sulfide analogues were found. The unit cell parameters of the title compound are $a = b = 14.3203(5)$ Å, $c = 9.7057(4)$ Å, and $Z = 3$. In an asymmetric unit of the title compound, K, Hg/Ga and Se occupy one, three, and four unique sites, respectively. The multivalent metal positions are disordered by Hg and Ga atoms with respective occupancies of 0.3 − 0.577 for Hg and 0.423 − 0.7 for Ga (More details are listed in Table 2). Since no intermetallic bonds or diselenide bonds exist in the structure, the common oxidation states of 1+, 2+, 3+ and 2– could be respectively distributed to K, Hg, Ga, and Se atoms. The calculated bond valence sums (BVS)[48] for all atoms (see Table 4) are in good accordance with the expected weighted average values, indicating the atom assignments are reasonable.

The overall structure of the title compound is shown in Figure 2a. Clearly, all Hg*N*/Ga*N* (*N* = 1, 2, 3) atoms are surrounded by four Se atoms to form (Hg*N*/Ga*N*)Se_4

(N = 1, 2, 3) tetrahedra with relatively large distortion (see Figure 3a, b, c), which are well aligned in an additive manner parallel to the *c* axis. These tetrahedra are first linked to each other by vertex-sharing to form a two-dimensional layer parallel to the *ab* plane (see Figure 2b), and then, the layers are stacked along the *c* axis to construct a overall three-dimensional framework with K^+ filling in the voids. Such a arrangement leads to a relatively large packing density of the NLO-active functional groups $(Hg/Ga)Se_4$. The basic repeating building unit of a constituent layer can be derived as a $(Hg/Ga)_9Se_{24}$ block, which contains three $(Hg1/Ga1)Se_4$ tetrahedra, three $(Hg2/Ga2)Se_4$ tetrahedra and three $(Hg3/Ga3)Se_4$ tetrahedra. The detailed connecting mode within a $(Hg/Ga)_9Se_{24}$ block is shown in Figure 2c. The Hg/Ga − Se bonds lengths and Se − Hg/Ga − Se angles are in the range of 2.444(3) − 2.571(2) Å and 100.37(9)° − 121.29(7)°, respectively, which are comparable with those observed in $HgGa_2Se_4$ (Hg − Se : 2.610(5) Å; Ga − Se : 2.403(2) Å and 2.409(0) Å; Se − Hg − Se : 109.17(6)° − 110.06(2)°; Se − Ga − Se : 103.21(3)° − 119.51(8)°).[49] The interstitial K atoms are bound to twelve Se atoms by weak electrostatic interactions (see Figure 3d), giving a cuboctahedron with four sets of K − Se distances (3.741(6) Å, 3.763(6) Å, 3.780(1) Å and 3.828(2) Å). These data are a little larger than the observed values of 3.335(9) − 3.586(3) Å in $K_2Sn_2ZnSe_6$,[50] and in good accordance with those in $KCd_4Ga_5Se_{12}$ (3.772(5) − 3.848(1) Å)[45] and $K_4GeP_4Se_{12}$ (3.265(4) − 3.903(4) Å).[51]

Structurally, the covalently bonded frameworks of $KHg_4Ga_5Se_{12}$ and its ternary prototype $HgGa_2Q_4$ (Q = S, Se) are both comprised of corner-sharing HgQ_4 and GaQ_4 tetrahedra. Nevertheless, some apparent structural differences can still be summarized:

(1) The Hg and Ga atoms in $HgGa_2Q_4$ occupy totally different positions, while in $KHg_4Ga_5Se_{12}$, the bivalent cation Hg and trivalent cation Ga are completely disordered. (2) The detailed stacking modes of the basic motifs differ greatly between these two compounds. For $HgGa_2Q_4$, it can be regarded as a derivative of the chalcopyrite-type compound $AgGaQ_2$: about half of the monovalent Ag^+ cations in $AgGaQ_2$ are substituted by the bivalent Hg^{2+} cations, leaving the other half of the mono-metallic sites being vacancies. As for $KHg_4Ga_5Se_{12}$, that the alkali metal K occupies one of the Se positions makes the arrangement of the Se atoms no longer a closest packing manner. Apart from their structural differences, it is worth noting that the sulfide $HgGa_2S_4$ has long been studied as promising IR NLO materials (the selenide $HgGa_2Se_4$ has not been studied in detail yet), however, it is extremely difficult to obtain high-quality large-size $HgGa_2S_4$ single crystals. For our compound $KHg_4Ga_5Se_{12}$, it exhibits much enhanced SHG response and longer transparent range compared with the sulfide $HgGa_2S_4$ (these properties will be discussed in detail in the next sections).

Raman Spectroscopy and UV-vis-NIR Diffuse Reflectance Spectroscopy. A Raman spectrum was recorded on the polycrystalline sample of $KHg_4Ga_5Se_{12}$ (Figure 4). Several obvious absorption peaks can be seen from 100 cm^{-1} to 500 cm^{-1}. The most distinct Raman shift at 196 cm^{-1} is attributed to the symmetric stretch of Hg − Se bonds, which is in good agreement with the observed 191 cm^{-1} peak in $Cs_2HgSn_3Se_8$.[52] The peaks at 328 cm^{-1} and 413 cm^{-1} can be assigned to Ga − Se absorption modes, agreeing well with the fact that the lighter weight of a atom always

results in a higher stretching frequency. Other absorptions below 200 cm^{-1} may arise from the K − Se vibrations.

The optical band gap of $KHg_4Ga_5Se_{12}$ was surveyed by the plot of F(*R*) (absorption data) versus *hv* (photon energy) based on the Kubelka-Munk equation.[53-56] As displayed in Figure 5, a sharp absorption edge appears at about 770 nm corresponding to a band gap of 1.61 eV, which is in good accordance with the 'dark-red' color of $KHg_4Ga_5Se_{12}$. In addition, it is worth noting that very little optical absorption emerges below the band gap, indicating the polycrystalline sample has high purity and the light transmission cross over the title compound has not been disturbed. Such a band gap is close to that of commercial $ZnGeP_2$ (1.75 eV) and $AgGaSe_2$ (1.80 eV) and makes the material suitable for the common 2 μm laser as pumping source for IR laser generation. The band gap is smaller than that of commercial sulfide $AgGaS_2$ (2.56 eV) and may not be beneficial for increasing the laser damage threshold. However, the laser damage threshold is also influenced by other factors such as chemical composition, the thermal conductivity, and crystal quality. For example, $ZnGeP_2$ demonstrates much larger laser damage threshold than $AgGaQ_2$ (Q = S, Se) do for 2 μm pumping sources. For the transparent edge in the IR range, the crystal currently obtained via the spontaneous nucleation method is too small for measuring the transmission spectrum in the mid-far IR range, but as a selenide containing heavy metal Hg, its IR transparent range can be up to 20 μm, significantly longer than those of the sulfide $HgGa_2S_4$ and $AgGaS_2$ as well as the phosphide $ZnGeP_2$ (around 13 μm). It is worthy noting that the search for NLO

materials in the far IR or even the terahertz range is becoming increasingly important.

Thermal Stability. The differential scanning calorimetric curve of $KHg_4Ga_5Se_{12}$ is shown in Figure 6. The material is stable up to 700□, then melts incongruently with two endothermic peaks at 742 □ and 781 □ and two exothermic peaks at 680 □ and 712 □ during the entire heating/cooling cycle. The DSC curve indicates that $KHg_4Ga_5Se_{12}$ has relatively high thermal stability.

SHG Properties. Owing to its structural asymmetry and favorable alignments of the functional groups, $KHg_4Ga_5Se_{12}$ is expected to exhibit strong SHG response. By applying the Kurtz–Perry method,[32] the powder SHG response of $KHg_4Ga_5Se_{12}$ has been studied in detail with a Q-switched Ho: Tm: Cr: YAG laser (2.09 μm, 3Hz, 50 ns). As shown in Figure 7a, the SHG intensities grow gradually as the particle size increase and then reach a plateau, indicating that the title compound is phase-matchable at the common 2 μm pumping sources. It should be emphasized that good phase-matchability is a highly desirable attribute for a IR NLO compound to become real applicable. Marvelously, if the SHG signals are compared at the same particle size range of 150 – 200 μm, the SHG response of $KHg_4Ga_5Se_{12}$ would be about 20 times that of the commercialized material $AgGaS_2$ (see Figure 7b). To our best knowledge, such a value is one of the largest responses among all the phase-matchable IR NLO chalcogenides reported to date. For comparison, the SHG responses of some promising phase-matchable materials $BaGa_4S_7$,[14] $Ba_6Zn_7Ga_2S_{16}$,[57] $Na_4MgGe_2Se_6$,[58] $NaGaIn_2Se_5$,[59] and $BaGa_4Se_7$[15] are only about 1.0, 1.0, 1.3, 2.1, 3.0 times that of $AgGaS_2$, respectively. Moreover, it is noteworthy that the Zn- and

Cd-containing analogues[45-47] have also been reported to exhibit large SHG efficiency, for example, by using the 2.05 μm pumping sources, the respective SHG responses of $RbZn_4In_5Se_{12}$, $CsZn_4In_5Se_{12}$ and $KCd_4Ga_5Se_{12}$ were experimentally determined as 26.7, 25.0 and 26.8 times that of $AgGaS_2$ at the particle size of 46 – 74 μm. However, all these analogues exhibit non phase-matchable feature with the maximum SHG intensity realized at the small particle size of 46 – 74 μm, resulting from the relatively low birefringence (*e.g.*, the static birefringence of $CsCd_4Ga_5S_{12}$, $CsCd_4Ga_5Se_{12}$ and $CsCd_4In_5Se_{12}$ at 2.05 μm were calculated as 0.003, 0.014 and 0.01, respectively). When compared at other larger particle size range (*e.g.*, 150 – 200 μm), the SHG responses of these analogues were significantly decreased (*e.g.*, the respective SHG intensities of $RbZn_4In_5Se_{12}$ and $CsZn_4In_5Se_{12}$ are only about 3.9 and 3.5 times that of $AgGaS_2$ at the particle size of 150 – 200 μm). But for our newly discovered compound $KHg_4Ga_5Se_{12}$, the introduction of the highly polarizable Hg−Se bonds with large susceptibility into the crystal structure of the title compound strengthen its anisotropic polarizability to a large extent, and thus exhibiting a favorable phase-matching feature (in other words, the SHG intensity of $KHg_4Ga_5Se_{12}$ increases as the particle size increases). As one may know, the birefringence (Δn) of a crystal is mainly decided by the anisotropic polarizability of its structure and a suitable birefringence is very practically profitable to achieve the phase-matching condition. From a structural point of view, the SHG response and birefringence of a crystal are closely related with the distortion degree and the packing density of the NLO-active functional groups. Basically, a dense packing and completely parallel alignment of the

functional groups with large distortion would lead to a large SHG response and a appreciable birefringence. Take $AZn_4In_5Se_{12}$ (A = Rb, Cs) and $KCd_4Ga_5Se_{12}$ for example, the Zn/In − Se and Cd/Ga − Se bond lengths are in the range of 2.511(4) − 2.545(4) Å, 2.458(2) − 2.554(2) Å, respectively, while in the case of $KHg_4Ga_5Se_{12}$, as discussed in the foregoing section, the Hg/Ga − Se bond lengths range from 2.444(3) to 2.571(2) Å. Clearly, the $(Hg/Ga)Se_4$ tetrahedra exhibit much more pronounced distortion than that $(Zn/In)Se_4$ and $(Cd/Ga)Se_4$ tetrahedra do, indicating that the Hg−Se bonds play a vital role in obtaining the phase-matching feature, while concurrently acquiring the large SHG efficiency. Additionally, considering the second-order coefficients of a compound are proportional to the square root of the SHG intensities, the corresponding coefficient of $KHg_4Ga_5Se_{12}$ can be derived as large as 58.1 pm/V, further suggesting the title compound may be used as a frequency converting material with very high efficiency.

Calculated Band Structure. The electronic band structure along the highly symmetrical path of $KHg_4Ga_5Se_{12}$ clearly demonstrate that the title compound is a direct transition semiconductor with the calculated energy band gap of 0.9 eV (see Figure 8). It is generally accepted that the calculated band gap should be a little smaller than the measured value due to the discontinuity of exchange-correlation energy. Therefore, the scissor operators were adopted to shift all the conduction bands to match the calculated band gap with the measured value. Meanwhile, Figure 9 displays the density of states (DOS) and the partial density of states (PDOS) projected on the constitutional atoms of the title compound. Accordingly, the following

electronic characteristics could be inferred: (1) The region lower than −7 eV is consisted of the isolated inner-shell states of the constitutional atoms (K 3*p*, Ga 3*d*, Hg 5*d* and Se 4*s* orbitals). These orbitals have little interaction with neighboring atoms and contribute very little to the optical properties of the title compound. (2) The upper part of VBs is mainly composed of the Hg 6*s*, Ga 4*s*4*p* and Se 4*p* orbitals, indicating that these atoms are involved in the formation of chemical bonding with relatively strong covalency. (3) The bottom part of CBs is dominated by the orbitals of all atoms. Since the optical behavior of a crystal mainly originates from the electronic transitions between the quantum states of the VBs and the CBs close to the band gap, the Hg/Ga-Se groups should be responsible for the linear and nonlinear optical properties of the compound, while the contribution from the alkali metal cation K^+ could be neglected.

First-principles Calculation of the Optical Properties. Being restricted by the Kleinman's symmetry rule, $KHg_4Ga_5Se_{12}$ should have four non-zero independent SHG coefficients (d_{11}, d_{15}, d_{22} and d_{33}) owing to its *R3* space group. The static SHG tenors (*i.e.*, obtained at input photon energy of 0.0 eV) are calculated as below: d_{11} = -44.945 pm/V, d_{15} = 45.238 pm/V, d_{22} = -42.481 pm/V, d_{33} = -65.257 pm/V. The maximum coefficient (d_{33} = -65.257 pm/V) agrees with the powder SHG determination (58.1 pm/V). Meanwhile, it should be mentioned that the SHG coefficients are related to the input photon energy. Basically, there is a positive correlation between the SHG coefficients and the frequencies of the input photons. However, within a relatively small energy region (*e.g.*, 0 − 0.593 eV, corresponding to

0 − 2090 nm), the change for the calculated values is small.[45] Hence, the above static values may still provide a approximate assessment about the experimental results. In order to gain a better understanding of the relationship between the optical properties and crystal structure of $KHg_4Ga_5Se_{12}$, a so-called real-space atom-cutting method was intend to be applied to assess the respective contribution of the functional anionic groups and cations to the SHG response. In the above method, the whole real space of the crystal cell is partitioned into several individual sphere zones corresponding to the respective ions (groups). The sizes of the sphere zones are mainly determined by the radius of the ions (the radii of the atoms contained in the groups). However, it should be noted that partially occupied structure (like the title compound) can not be used directly for the atom-cutting analysis. To make the atom-cutting analysis operable, several different configurations of the structure are designed in the symmery of *P*1, where twelve Hg and fifteen Ga cations are randomly distributed over the twenty-seven 9*b* Wyckoff positions with 100% occupancy. By calculating the respective energy of these configurations, the most energy favorable one was identified. Then the real-space atom-cutting technique was conducted on this designed model. As shown in Table 5, the maximum coefficient d_{33} is -0.898 pm/V for K^+ (1.4% of d_{33}) and -63.938 pm/V for $(Hg/Ga)Se_4$ (98.6% of d_{33}). This verifies the band structure analysis very well and further demonstrate that the origin of the SHG response of $KHg_4Ga_5Se_{12}$ mainly arise from the $(Hg/Ga)Se_4$ chromophores. To intuitive see the origin of the macroscopic SHG response of $KHg_4Ga_5Se_{12}$, the SHG-weighted densities of the occupied (see Figure 10a) and unoccupied electronic

states (see Figure 10b) have been calculated. Obviously, the (Hg/Ga)Se_4 groups are the major source of the SHG-weighted electron densities in both occupied and unoccupied states. This result further indicates that the $HgSe_4$ and $GaSe_4$ chromophores make the definitive contributions for the nonlinear optical properties of the title compound.

It is generally accepted that, in a polar compound, the magnitude and direction of the local dipole moments of the functional groups determine the macroscopic SHG effects. To make the origin of the SHG response more clear, we have also quantified the local dipole moments of the Hg/Ga − Se groups for $KHg_4Ga_5Se_{12}$ with a simple bond-valence method as described previously.[60,61] As calculated, the *x* and *y* components of the polarizations from all groups cancelled each other to zero, while a net dipole moment remained along the *z* direction, which is in accordance with the symmetry of its specific space group (*R*3). The *z* component of the static dipole moments of different groups (Hg1/Ga1)Se_4, (Hg2/Ga2)Se_4 and (Hg3/Ga3)Se_4 are -0.48 D, -0.11 D and 0.57 D, respectively. Considering a unit cell of the title compound contains twenty-seven such tetrahedra, thus, the corresponding local dipole moment of a unit cell would be -0.18 D. Such a remanent value is responsible for the large SHG efficiency of $KHg_4Ga_5Se_{12}$.

Furthermore, the dispersion curves of the refractive indexes for $KHg_4Ga_5Se_{12}$ are depicted in Figure 11. On account of its specific symmetry, the title compound has two independent refractive indexes ($n_x = n_y$, and n_z). The derived birefringence (Δn) at 1.06 μm and 2.09 μm are calculated as 0.054 and 0.072, respectively. Generally, good

IR phase-matchability of a crystal normally require a moderate birefringence (0.04 – 0.10).[62] The too small birefringence ($\Delta n < 0.04$) is not adequate to achieve the phase-matching condition, while the too large birefringence ($\Delta n > 0.10$) may lead to some destructive optical behaviors. The calculated Δn value at 2.09 μm (0.072) indicates the title compound is likely to be phase-matchable, which corroborates the experimental observation very well. Particularly, although the title compound may be not suitable for the 1.06 μm laser as pumping source for IR laser generation due to its relatively narrow band gap, the calculated birefringence at 1.06 μm (0.054) still suggests that this material has very strong anisotropic polarizability at this specific wavelength. Hence, one may conclude that the introduction of the highly polarizable Hg−chalcogens bonds into a crystal structure would be an effective pathway to fulfill the phase-matchable requirements, while simultaneously acquiring large SHG efficiency.

CONCLUSION

To sum up, a new Hg-based infrared nonlinear optical material $KHg_4Ga_5Se_{12}$ has been synthesized and characterized. Its three-dimensional framework is composed of corner-sharing $HgSe_4$ and $GaSe_4$ tetrahedra with the counter-ion K^+ filling in the voids. Though $KHg_4Ga_5Se_{12}$ and its ternary prototype $HgGa_2Se_4$ have similar covalent structure, the cation occupancies and the detailed stacking modes of the basic motifs differ greatly between these two compounds. For this new material, it is very interesting that all the NLO-active chromophores ($HgSe_4$ and $GaSe_4$ tetrahedra) are

arranged in a completely cooperative manner. The introduction of the highly polarizable Hg-Se bond can induce more pronounced distortion in the tetrahedral building units, and strengthen its anisotropic polarizability to a large extent, and thus result in a favorable phase-matching feature along with very large SHG response. According to the diffuse reflectance spectrum and electronic structure calculation, $KHg_4Ga_5Se_{12}$ is characterized as a direct transition semiconductor with the band gap of 1.61 eV. Moreover, the electronic band structure, the real-space atom-cutting analysis, together with the SHG-weighted electronic densities and the local dipole moments calculations reveal that the origin of the excellent linear and nonlinear optical properties of $KHg_4Ga_5Se_{12}$ can be ascribed to the $(Hg/Ga)Se_4$ group. These competitive features (good phase-matchability, very large SHG efficiency, wide transparency) make our newly discovered compound $KHg_4Ga_5Se_{12}$ a promising IR NLO material. Furthermore, this study further corroborates our consideration that Hg-based metal chalcogenides may be used as promising alternatives for IR NLO optics and may provide some insights for further exploration of IR NLO materials. Further effort, *i.e.*, growth on large-size single crystal for comprehensive assessment of this new IR NLO material is ongoing.

ASSOCIATED CONTENT

Supporting Information

The crystallographic file in CIF format for $KHg_4Ga_5Se_{12}$. This material is available free of charge via the Internet at http://pubs.acs.org.

ACKNOWLEDGMENTS

This research was supported by National Natural Science Foundation of China (No. 21271178, No. 51472251 and No. 91622123).

Figure Captions

Figure 1 The experimental powder X–ray diffraction pattern (red) and simulated pattern (black) of $KHg_4Ga_5Se_{12}$.

Figure 2 (a) The crystal structure of $KHg_4Ga_5Se_{12}$, in which a constituent layer is marked with a black dashed border. Tetrahedra: $(Hg/Ga)Se_4$. (b) A single two-dimensional layer parallel to the *ab* plane. (c) The basic repeating building unit, $(Hg/Ga)_9Se_{24}$, with the detailed atom numbers marked. 1: Hg1/Ga1; 2: Hg2/Ga2; 3: Hg3/Ga3.

Figure 3 The detailed coordination environment of (a) Hg1/Ga1; (b) Hg2/Ga2; (c) Hg3/Ga3; (d) K^+.1: Hg1/Ga1; 2: Hg2/Ga2; 3: Hg3/Ga3.

Figure 4 Raman spectrum of $KHg_4Ga_5Se_{12}$.

Figure 5 The UV-vis-NIR diffuse reflectance spectrum of $KHg_4Ga_5Se_{12}$.

Figure 6 The differential scanning calorimetric curve of $KHg_4Ga_5Se_{12}$.

Figure 7 (a) The phase-matching curve, i.e., SHG response versus particle size, for $KHg_4Ga_5Se_{12}$. (b) Oscilloscope traces of SHG signals of $KHg_4Ga_5Se_{12}$ and $AgGaS_2$ (reference) in the particle size of 150 – 200 μm.

Figure 8 Electron band structure along highly symmetrical path in Brillouin zone of $KHg_4Ga_5Se_{12}$.

Figure 9 The partial density of states (PDOS) projected onto the constituted atoms of $KHg_4Ga_5Se_{12}$.

Figure 10 SHG-weighted densities for the (a) occupied and (b) unoccupied electronic states in $KHg_4Ga_5Se_{12}$.

Figure 11 The dispersion curves of the refractive indexes for $KHg_4Ga_5Se_{12}$ in the range of 700 – 3500 nm.

REFERENCES

(1) Petrov, V. Parametric down-conversion devices: The coverage of the mid-infrared spectral range by solid-state laser sources. *Opt. Mater.* **2012**, *34*, 536-554.

(2) Hu, C. L.; Mao, J. G. Recent advances on second-order NLO materials based on metal iodates. *Coord. Chem. Rev.* **2015,** *288*, 1-17.

(3) Mao, F. F.; Hu, C. L.; Xu, X.; Yan, D.; Yang, B. P.; Mao, J. G. $Bi(IO_3)F_2$: The First Metal Iodate Fluoride with a Very Strong Second Harmonic Generation Effect. *Angew. Chem. Int. Edit.* **2017,** *56*, 2151-2155.

(4) Liang, M. L.; Hu, C. L.; Kong, F.; Mao, J. G. $BiFSeO_3$: An Excellent SHG Material Designed by Aliovalent Substitution. *J. Am. Chem. Soc.* **2016,** *138*, 9433-9436.

(5) Yin, W. L.; Iyer, A. K.; Li, C.; Yao, J. Y.; Mar, A. Noncentrosymmetric chalcogenides $BaZnSiSe_4$ and $BaZnGeSe_4$ featuring one-dimensional structures. *J. Alloys Compd.* **2017,** *708*, 414-421.

(6) Yin, W. L.; Iyer, A. K.; Li, C.; Yao, J. Y.; Mar, A. $Ba_5CdGa_6Se_{15}$, a congruently-melting infrared nonlinear optical material with strong SHG response. *J. Mater. Chem. C* **2017,** *5*, 1057-1063.

(7) Harasaki, A.; Kato, K. New data on the nonlinear optical constant, phase-matching, and optical damage of $AgGaS_2$. *Jpn. J. Appl. Phys.* **1997**, *36*, 700-703.

(8) Catella, G. C.; Shiozawa, L. R.; Hietanen, J. R.; Eckardt, R. C.; Route, R. K.; Feigelson, R. S.; Cooper, D. G.; Marquardt, C. L. Mid-IR Absorption in $AgGaSe_2$ Optical Parametric Oscillator Crystals. *Appl. Opt.* **1993**, *32*, 3948-3951.

(9) Boyd, G. D.; Buehler, E.; Storz, F. G. Linear and Nonlinear Optical Properties of $ZnGeP_2$ and CdSe. *Appl. Phys. Lett.* **1971**, *18*, 301-304.

(10) Isaenko, L.; Yelisseyev, A.; Lobanov, S.; Titov, A.; Petrov, V.; Zondy, J. J.; Krinitsin, P.; Merkulov, A.; Vedenyapin, V.; Smirnova, J. Growth and properties of

$LiGaX_2$ (X = S, Se, Te) single crystals for nonlinear optical applications in the mid-IR. *Cryst. Res. Technol.* **2003**, *38*, 379-387.

(11) Isaenko, L.; Vasilyeva, I.; Yelisseyev, A.; Lobanov, S.; Malakhov, V.; Dovlitova, L.; Zondy, J. J.; Kavun, I. Growth and characterization of $LiInS_2$ single crystals. *J. Cryst. Growth* **2000**, *218*, 313-322.

(12) Badikov, V. V.; Chizhikov, V. I.; Efimenko, V. V.; Efimenko, T. D.; Panyutin, V. L.; Shevyrdyaeva, G. S.; Scherbakov, S. I. Optical properties of lithium indium selenide. *Opt. Mater.* **2003**, *23*, 575-581.

(13) Bera, T. K.; Jang, J. I.; Song, J. H.; Malliakas, C. D.; Freeman, A. J.; Ketterson, J. B.; Kanatzidis, M. G. Soluble Semiconductors $AAsSe_2$ (A = Li, Na) with a Direct-Band-Gap and Strong Second Harmonic Generation: A Combined Experimental and Theoretical Study. *J. Am. Chem. Soc.* **2010,** *132*, 3484-3495.

(14) Lin, X.; Zhang, G.; Ye, N. Growth and Characterization of $BaGa_4S_7$: A New Crystal for Mid-IR Nonlinear Optics. *Cryst. Growth Des.* **2009**, *9*, 1186-1189.

(15) Yao, J.; Mei, D.; Bai, L.; Lin, Z.Yin, W.; Fu, P.; Wu, Y. $BaGa_4Se_7$: A New Congruent-Melting IR Nonlinear Optical Material. *Inorg. Chem.* **2010**, *49*, 9212-9216.

(16) Luo, Z. Z.; Lin, C. S.; Cui, H. H.; Zhang, W. L.; Zhang, H.; He, Z. Z.; Cheng, W. D. SHG Materials $SnGa_4Q_7$ (Q = S, Se) Appearing with Large Conversion Efficiencies, High Damage Thresholds, and Wide Transparencies in the Mid-Infrared Region. *Chem. Mater.* **2014**, *26*, 2743−2749.

(17) Wu, K.; Yang, Z. H.; Pan, S. L. Na_2BaMQ_4 (M = Ge, Sn; Q = S, Se): Infrared Nonlinear Optical Materials with Excellent Performances and that Undergo Structural Transformations. *Angew. Chem. Int. Edit.* **2016**, *55*, 6712-6714.

(18) Chen, M. C.; Wu, L. M.; Lin, H.; Zhou, L. J.; Chen, L. Disconnection Enhances the Second Harmonic Generation Response: Synthesis and Characterization of

$Ba_{23}Ga_8Sb_2S_{38}$. *J. Am. Chem. Soc.* **2012**, *134*, 6058-6060.

(19) Liu, B. W.; Zeng, H. Y.; Zhang, M. J.; Fan, Y. H.; Guo, G. C.; Huang, J. S.; Dong, Z. C. Syntheses, Structures, and Nonlinear-Optical Properties of Metal Sulfides $Ba_2Ga_8MS_{16}$ (M = Si, Ge). *Inorg. Chem.* **2015**, *54*, 976-981.

(20) Atuchin, V. V.; Kesler, V. G.; Ursaki, V. V.; Tezlevan, V. E. Electronic structure of $HgGa_2S_4$. *Solid State Commun.* **2006**, *138*, 250-254.

(21) Wu, K.; Su, X.; Pan, S. L.; Yang, Z. H. Synthesis and Characterization of Mid-Infrared Transparency Compounds: Acentric $BaHgS_2$ and Centric $Ba_8Hg_4S_5Se_7$. *Inorg. Chem.* **2015**, *54*, 2772-2779.

(22) Li, C.; Yin, W. L.; Gong, P. F.; Li, X. S.; Zhou, M. L.; Mar, A.; Lin, Z. S.; Yao, J. Y.; Wu, Y. C.; Chen, C. T. Trigonal Planar $[HgSe_3]^{4-}$ Unit: A New Kind of Basic Functional Group in IR Nonlinear Optical Materials with Large Susceptibility and Physicochemical Stability. *J. Am. Chem. Soc.* **2016**, *138*, 6135-6138.

(23) Wu, K.; Pan, S. L. Li_2HgMS_4 (M = Si, Ge, Sn): New Quaternary Diamond-Like Semiconductors for Infrared Laser Frequency Conversion. *Crystals* **2017,** *7*, 107-118.

(24) Wu, K.; Yang, Z. H.; Pan, S. L. The first quaternary diamond-like semiconductor with 10-membered LiS_4 rings exhibiting excellent nonlinear optical performances. *Chem. Commun.* **2017,** *53*, 3010-3013.

(25) Liao, J. H.; Marking, G. M.; Hsu, K. F.; Matsushita, Y.; Ewbank, M. D.; Borwick, R.; Cunningham, P.; Rosker, M. J.; Kanatzidis, M. G. α- and β-$A_2Hg_3M_2S_8$ (A = K, Rb; M = Ge, Sn): Polar quaternary chalcogenides with strong nonlinear optical response. *J. Am. Chem. Soc.* **2003**, *125*, 9484-9493.

(26) Wu, K.; Yang, Z. H.; Pan, S. L. $Na_2Hg_3M_2S_8$ (M = Si, Ge, and Sn): New Infrared Nonlinear Optical Materials with Strong Second Harmonic Generation Effects and High Laser-Damage Thresholds. *Chem. Mater.* **2016**, *28*, 2795-2801.

(27) Fang, A. H.; Huang, F. Q.; Xie, X. M.; Jiang, M. H. Low-Temperature Rapid

Synthesis and Superconductivity of Fe-Based Oxypnictide Superconductors. *J. Am. Chem. Soc.* **2010**, *132*, 3260-3261.

(28) Yin, W. L.; Iyer, A. K.; Lin, X. S.; Mar, A. $Ba_4Ga_2Se_8$: A ternary selenide containing chains and discrete Se_2^{2-} units. *J. Solid State Chem.* **2016,** *237*, 144-149.

(29) Zhang, S. Y.; Mei, D. J.; Du, X.; Lin, Z. S.; Zhong, J. B.; Wu, Y. D.; Xu, J. L. The structure and band gap design of high Si doping level $Ag_{1-x}Ga_{1-x}Si_xSe_2$ (x = 1/2). *J. Solid State Chem.* **2016,** *238*, 21-24.

(30) CrysAlispro, version 1.171.35.11, Agilent Technologies, 2012.

(31) Sheldrick, G. M. A short history of SHELX. *Acta. Crystallogr.*, *Sect. A: Found. Crystallogr.* **2008**, *64*, 112-122.

(32) Kurtz, S. K.; Perry, T. T. A Powder Technique for Evaluation of Nonlinear Optical Materials. *J. Appl. Phys.* **1968**, *39*, 3798-3813.

(33) Clark, S. J.; Segall, M. D.; Pickard, C. J.; Hasnip, P. J.; Probert, M. J.; Refson, K.; Payne, M. C. First principles methods using CASTEP. *Kristallogr.* **2005**, *220*, 567-570.

(34) Payne, M. C.; Teter, M. P.; Allan, D. C.; Arias, T. A.; Joannopoulos, J. D. Iterative Minimization Techniques for ab Initio Total-Energy Calculations: Molecular-Dynamics and Conjugate Gradients. *Rev. Mod. Phys.* **1992**, *64*, 1045-1097.

(35) Perdew, J. P.; Zunger, A. Self-Interaction Correction to Density-Functional Approximations for Many-Electron Systems. *Phys. Rev. B* **1981**, *23*, 5048-5079.

(36) Ceperley, D. M.; Alder, B. J. Ground-State of the Electron-Gas by a Stochastic Method. *Phys. Rev. Lett.* **1980**, *45*, 566-569.

(37) Rappe, A. M.; Rabe, K. M.; Kaxiras, E.; Joannopoulos, J. D. Optimized Pseudopotentials. *Phys. Rev. B* **1990**, *41*, 1227-1230.

(38) Kleinman, L.; Bylander, D. M. Efficacious Form for Model Pseudopotentials. *Phys. Rev. Lett.* **1982**, *48*, 1425-1428.

(39) Monkhorst, H. J.; Pack, J. D. Special Points for Brillouin-Zone Integrations. *Phys. Rev. B* **1976**, *13*, 5188-5192.

(40) Godby, R. W.; Schluter, M.; Sham, L. J. Self-Energy Operators and Exchange-Correlation Potentials in Semiconductors. *Phys. Rev. B* **1988**, *37*, 10159-10175.

(41) Palik, E. D. *Handbook of Optical Constants of Solids*. Academic Press: New York, **1985**.

(42) Lin, J.; Lee, M. H.; Liu, Z. P.; Chen, C. T.; Pickard, C. J. Mechanism for linear and nonlinear optical effects in β-BaB_2O_4 crystals. *Phys. Rev. B* **1999**, *60*, 13380-13389.

(43) Lin, Z. S.; Jiang, X. X.; Kang, L.; Gong, P. F.; Luo, S. Y.; Lee, M. H. First-principles materials applications and design of nonlinear optical crystals. *J. Phys. D: Appl. Phys.* **2014**, *47*, 1-19.

(44) Schwer, H.; Keller, E.; Kramer, V. Crystal Structure and Twinning of $KCd_4Ga_5S_{12}$ and Some Isotypic $AB_4C_5X_{12}$ Compounds. *Kristallogr.* **1993,** *204*, 203-213.

(45) Lin, H.; Chen, L.; Zhou, L. J.; Wu, L. M. Functionalization Based on the Substitutional Flexibility: Strong Middle IR Nonlinear Optical Selenides $AX^{II}_4X^{III}_5Se_{12}$. *J. Am. Chem. Soc.* **2013**, *135*, 12914-12921.

(46) Lin, H.; Zhou, L. J.; Chen, L. Sulfides with Strong Nonlinear Optical Activity and Thermochromism: $ACd_4Ga_5S_{12}$ (A = K, Rb, Cs). *Chem. Mater.* **2012**, *24*, 3406-3414.

(47) Lin, H.; Zheng, Y. J.; Hu, X. N.; Chen, H.; Yu, J. S.; Wu, L. M. Two New Non-centrosymmetric Selenides $AZn_4In_5Se_{12}$ (A = Rb, Cs): Synthesis, Characterization and Nonlinear Optical Properties. *Chem. Asian J.* **2017**, *12*, 453-458.

(48) Brown, I. D.; Altermatt, D. Bond-Valence Parameters Obtained from a

Systematic Analysis of the Inorganic Crystal-Structure Database. Acta Crystallogr., B **1985**, *41*, 244-247.

(49) Gastaldi, L.; Simeone, M. G.; Viticoli, S. Cation Ordering and Crystal-Structures in AGa_2X_4 Compounds ($CoGa_2S_4$, $CdGa_2S_4$, $CdGa_2Se_4$, $HgGa_2Se_4$, $HgGa_2Te_4$). *Solid State Commun.* **1985**, *55*, 605-607.

(50) Zhou, M. L.; Li, C.; Li, X. S.; Yao, J. Y.; Wu, Y. C. $K_2Sn_2ZnSe_6$, $Na_2Ge_2ZnSe_6$, and $Na_2In_2GeSe_6$: a new series of quaternary selenides with intriguing structural diversity and nonlinear optical properties. *Dalton Trans.* **2016**, *45*, 7627-7633.

(51) Morris, C. D.; Chung, I.; Park, S.; Harrison, C. M.; Clark, D. J.; Jang, J. I.; Kanatzidis, M. G. Molecular Germanium Selenophosphate Salts: Phase-Change Properties and Strong Second Harmonic Generation. *J. Am. Chem. Soc.* **2012**, *134*, 20733-20744.

(52) Morris, C. D.; Li, H.; Jin, H.; Malliakas, C. D.; Peters, J. A.; Trikalitis, P. N.; Freeman, A. J.; Wessels, B. W.; Kanatzidis, M. G. $Cs_2M^{II}M^{IV}{}_3Q_8$ (Q = S, Se, Te): An Extensive Family of Layered Semiconductors with Diverse Band Gaps. *Chem. Mater.* **2013**, *25*, 3344-3356.

(53) Simmons, E. L. Diffuse Reflectance Spectroscopy: Comparison of Theories *Appl. Opt.* **1975**, *14*, 1380-1386.

(54) Huang, H. W.; Han, X.; Li, X. W.; Wang, S. C.; Chu, P. K.; Zhang, Y. H. Fabrication of Multiple Heterojunctions with Tunable Visible-Light-Active Photocatalytic Reactivity in BiOBr-BiOI Full-Range Composites Based on Microstructure Modulation and Band Structures. *ACS Appl. Mat. Interfaces* **2015,** *7*, 482-492.

(55) Huang, H. W.; Chen, G.; Zhang, Y. H. Two Bi-based phosphate photocatalysts: Crystal structure, optical property and photocatalytic activity. *Inorg. Chem. Commun.* **2014,** *44*, 46-49.

(56) Huang, H. W.; He, Y.; Lin, Z. S.; Kang, L.; Zhang, Y. H. Two Novel Bi-Based Borate Photocatalysts: Crystal Structure, Electronic Structure, Photoelectrochemical Properties, and Photocatalytic Activity under Simulated Solar Light Irradiation. *J. Phys. Chem. C* **2013,** *117*, 22986-22994.

(57) Li, Y. Y.; Liu, P. F.; Wu, L. M. $Ba_6Zn_7Ga_2S_{16}$: A Wide Band Gap Sulfide with Phase-Matchable Infrared NLO Properties. *Chem. Mater.* **2017,** *29*, 5259-5266.

(58) Wu, K.; Yang, Z. H.; Pan, S. L. $Na_4MgM_2Se_6$ (M = Si, Ge): The First Noncentrosymmetric Compounds with Special Ethane-like $[M_2Se_6]^{6-}$ Units Exhibiting Large Laser-Damage Thresholds. *Inorg. Chem.* **2015,** *54*, 10108-10110.

(59) Li, S. F.; Jiang, X. M.; Liu, B. W.; Yan, D.; Lin, C. S.; Zeng, H. Y.; Guo, G. C. Superpolyhedron-Built Second Harmonic Generation Materials Exhibit Large Mid-Infrared Conversion Efficiencies and High Laser Induced Damage Thresholds. *Chem. Mater.* **2017,** *29*, 1796-1804.

(60) Izumi, H. K.; Kirsch, J. E.; Stern, C. L.; Poeppelmeier, K. R. Examining the out-of-center distortion in the $[NbOF_5]^{2-}$ anion. *Inorg. Chem.* **2005,** *44*, 884-895.

(61) Maggard, P. A.; Nault, T. S.; Stern, C. L.; Poeppelmeier, K. R. Alignment of acentric $MoO_3F_3^{3-}$ anions in a polar material: $(Ag_3MoO_3F_3(Ag_3MoO_4)Cl$. *J. Solid State Chem.* **2003,** *175*, 27-33.

(62) Kang, L.; Zhou, M. L.; Yao, J. Y.; Lin, Z. S.; Wu, Y. C.; Chen, C. T. Metal Thiophosphates with Good Mid-infrared Nonlinear Optical Performances: A First-Principles Prediction and Analysis. *J. Am. Chem. Soc.* **2015,** *137*, 13049-13059.

Figure 1

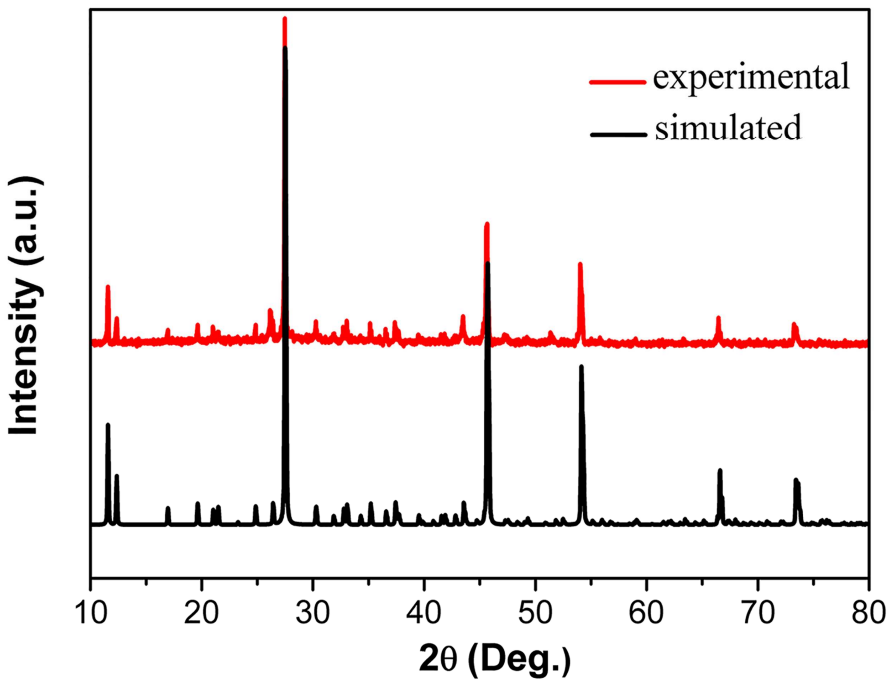
experimental
simulated
Intensity (a.u.)
10
20
30
40
50
60
70
80
2θ (Deg.)

Figure 2

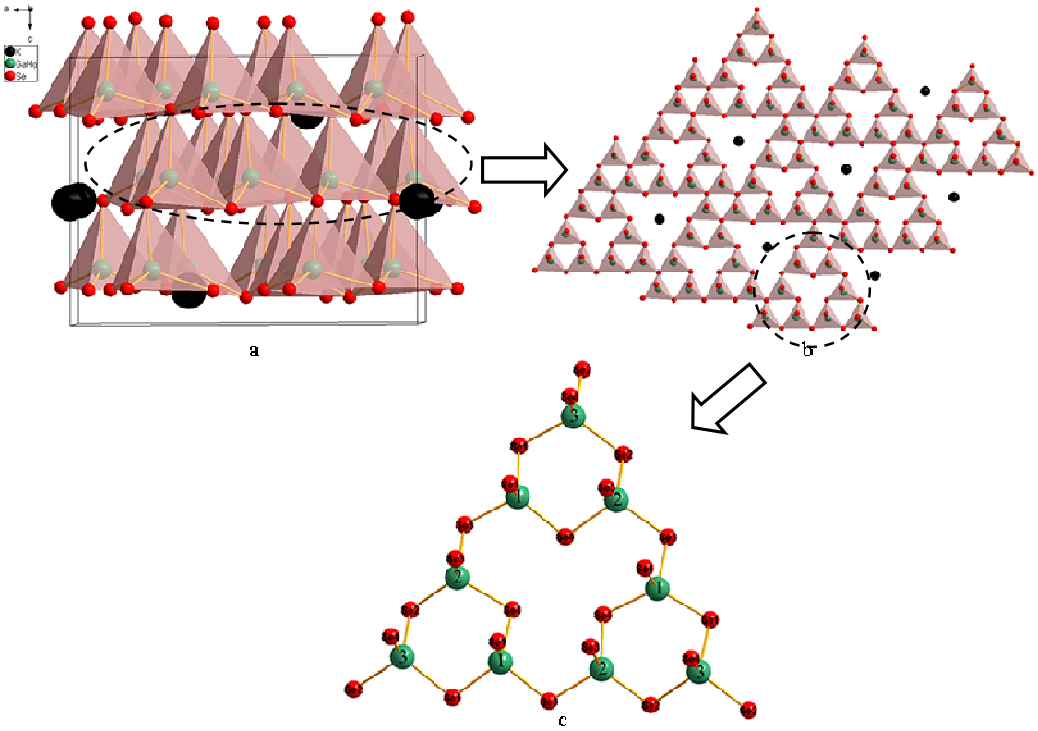

Figure 3

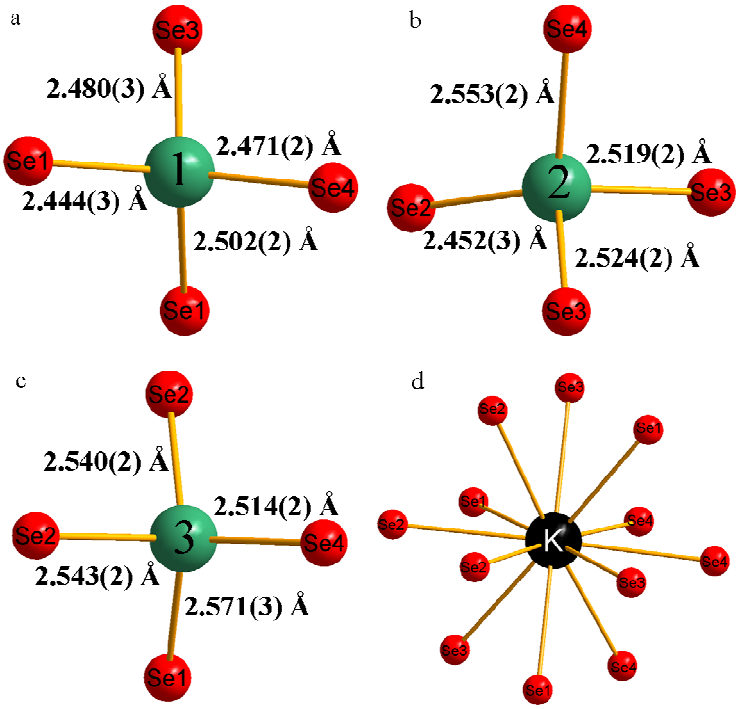
a
Se3
2.480(3) Å
Se1
1
2.471(2) Å
Se4
2.444(3) Å
2.502(2) Å
Se1
b
Se4
2.553(2) Å
2.519(2) Å
Se2
2
Se3
2.452(3) Å
2.524(2) Å
Se3
c
Se2
2.540(2) Å
2.514(2) Å
Se2
3
Se4
2.543(2) Å
2.571(3) Å
Se1
d
Se3
Se2
Se1
Se1
Se2
K
Se4
Se2
Se4
Se3
Se3
Se4
Se1

Figure 4

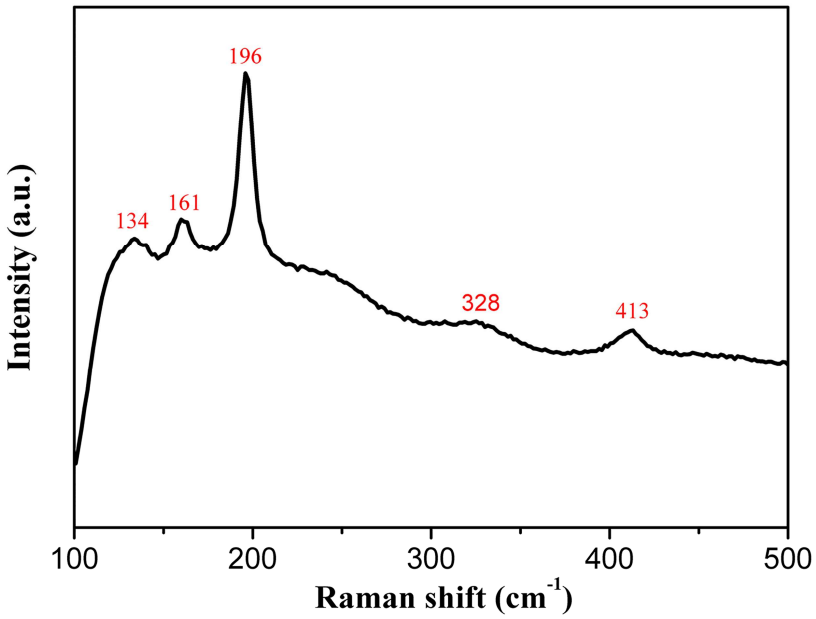
196
134
161
328
413
Intensity (a.u.)
100
200
300
400
500
Raman shift (cm-1)

Figure 5

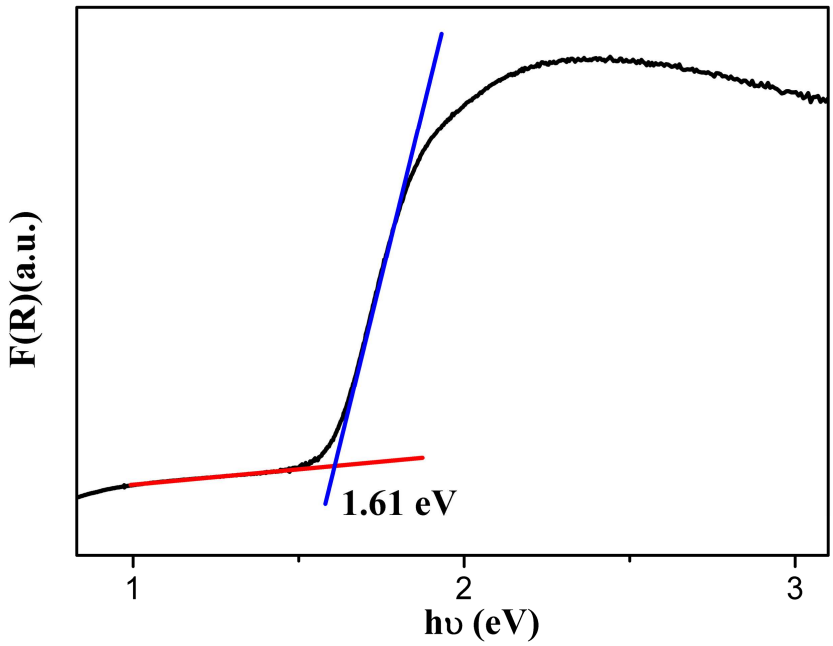

Figure 6

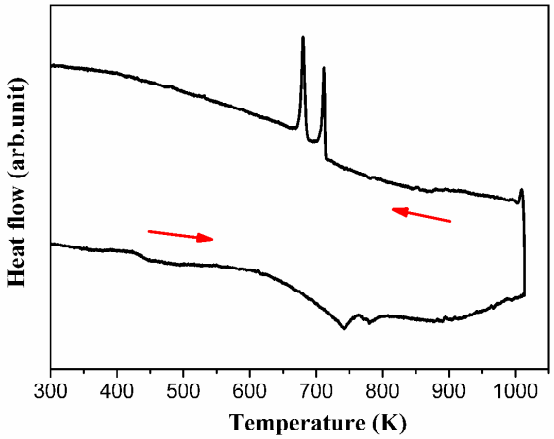
Heat flow (arb.unit)
300
400
500
600
700
800
900
1000
Temperature (K)

Figure 7

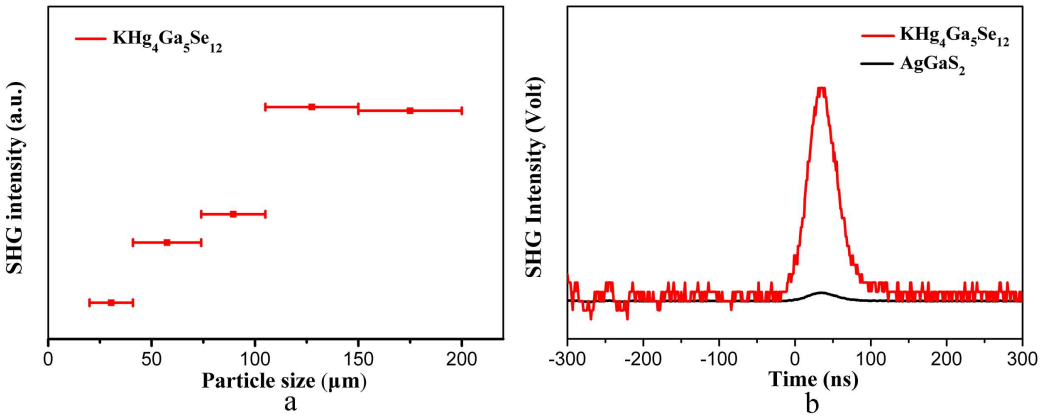
KHg4Ga5Se12
SHG intensity (a.u.)
0
50
100
150
200
Particle size (μm)
a
KHg4Ga5Se12
AgGaS2
SHG Intensity (Volt)
-300
-200
-100
0
100
200
300
Time (ns)
b

Figure 8

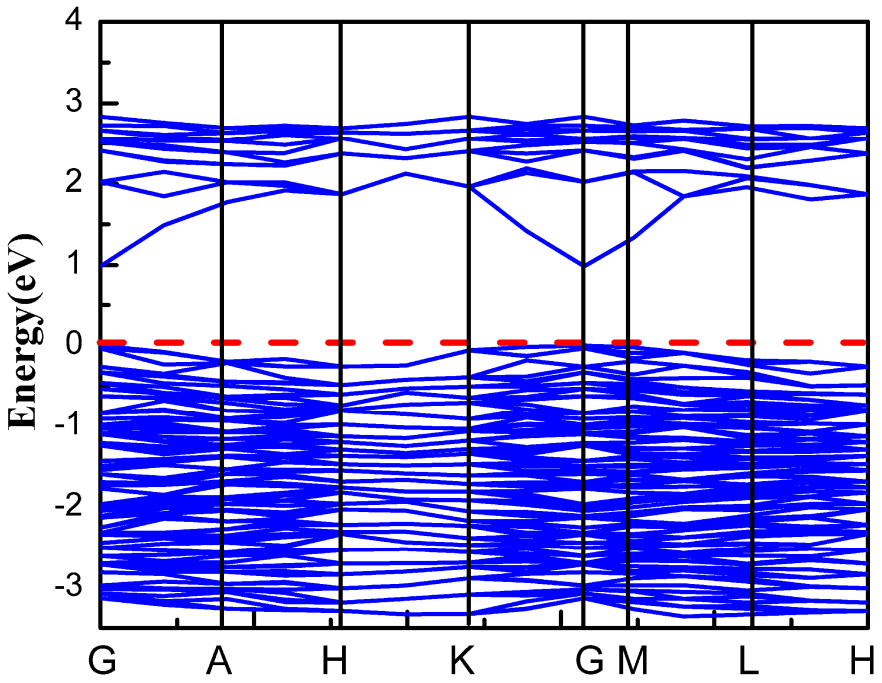

Figure 9

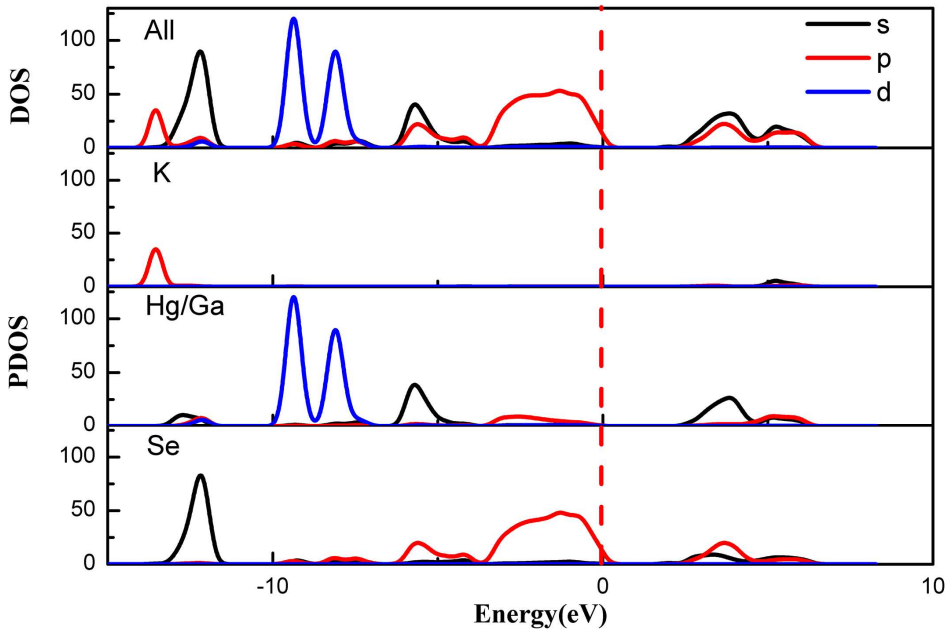

Figure 10

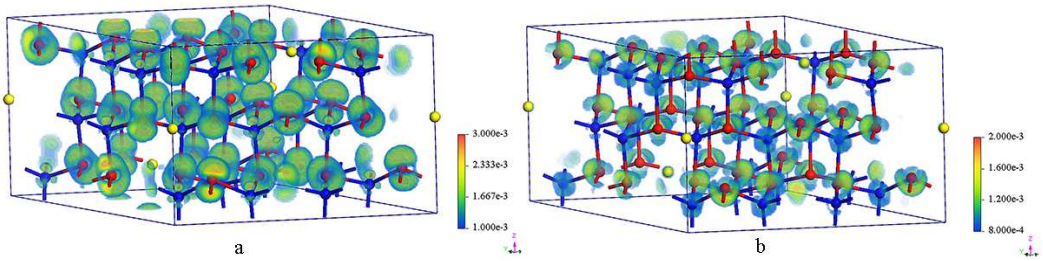
3.000e-3
2.333e-3
1.667e-3
1.000e-3
a
2.000e-3
1.600e-3
1.200e-3
8.000e-4
b

Figure 11

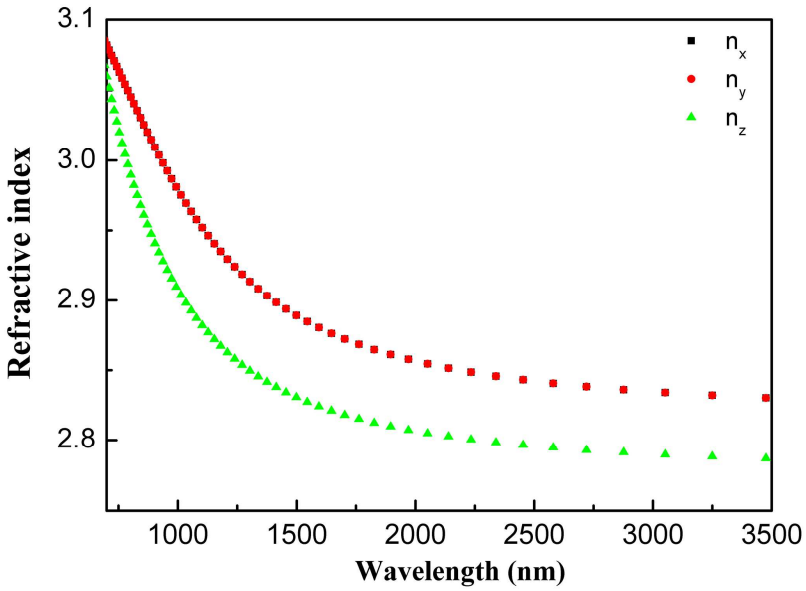
3.1
3.0
2.9
2.8
Refractive index
1000
1500
2000
2500
3000
3500
Wavelength (nm)
n_x
n_y
n_z

Table 1. Crystal data and structure refinement for $KHg_4Ga_5Se_{12}$.

Chemial content	**$KHg_4Ga_5Se_{12}$**
Fw	2137.58
a(Å)	14.3203(5)
b(Å)	14.3203(5)
c(Å)	9.7057(4)
γ (°)	120.00
Space group	$R3$
V(Å^3)	1723.7(1)
Z	3
T(K)	293(2)
λ(Å)	0.7107
ρ_c(g/cm^3)	6.178
μ(mm^{-1})	51.547
$R(F)$ [a]	0.0434
$R_W(F_o^2)$ [b]	0.0905
Flack parameter	-0.05(3)

[a] $R(F) = \Sigma \mid |F_o| - |F_c| \mid / \Sigma |F_o|$ for $F_o^2 > 2\sigma(F_o^2)$. [b] $R_W(F_o^2) = \{\Sigma [w(F_o^2 - F_c^2)^2] / \Sigma w F_o^4\}^{1/2}$ for all data. $w^{-1} = \sigma^2(F_o^2) + (zP)^2$, where $P = (\mathrm{Max}(F_o^2, 0) + 2F_c^2)/3$.

Table 2. Positional coordinates and equivalent isotropic displacement parameters for $KHg_4Ga_5Se_{12}$.

Atom	Wyckoff	x/a	y/b	z/c	U_{eq} [Å^2]	Occupancy
K	3*a*	0.0000	0.0000	0.5403(7)	0.0287(2)	1.000
Hg1/Ga1	9*b*	0.0996(1)	0.7400(6)	0.4626(7)	0.0073(4)	0.300/0.700
Hg2/Ga2	9*b*	0.4132(4)	0.9821(4)	0.4607(0)	0.0096(3)	0.456/0.544
Hg3/Ga3	9*b*	0.7948(3)	0.5133(6)	0.4534(4)	0.0100(2)	0.577/0.423
Se1	9*b*	0.9227(3)	0.7060(5)	0.5392(8)	0.0179(4)	1.000
Se2	9*b*	0.5399(2)	0.1551(0)	0.5677(0)	0.0194(4)	1.000
Se3	9*b*	0.2242(0)	0.9284(3)	0.5357(6)	0.0182(4)	1.000
Se4	9*b*	0.4503(6)	0.8314(7)	0.5285(1)	0.0136(3)	1.000

Table 3. Selected bond lengths(Å) for $KHg_4Ga_5Se_{12}$.

$KHg_4Ga_5Se_{12}$	
Hg1/Ga1—Se1	2.444(3)
Hg1/Ga1—Se4	2.471(3)
Hg1/Ga1—Se3	2.480(2)
Hg1/Ga1—Se1	2.502(2)
Hg2/Ga2—Se2	2.452(2)
Hg2/Ga2—Se3	2.519(2)
Hg2/Ga2—Se3	2.524(3)
Hg2/Ga2—Se4	2.553(3)
Hg3/Ga3—Se4	2.514(2)
Hg3/Ga3—Se2	2.540(3)
Hg3/Ga3—Se2	2.543(2)
Hg3/Ga3—Se1	2.571(2)
K—Se2	3.741(6)×3
K—Se4	3.763(6)×3
K—Se1	3.780(1)×3
K—Se3	3.828(2)×3

Table 4. Calculated bond valence sums for $KHg_4Ga_5Se_{12}$.

site	expected weighted averages	bond valence sums
K	1	0.711
Hg1/Ga1	2.7	2.856
Hg2/Ga2	2.544	2.754
Hg3/Ga3	2.423	2.656
Se1	-2	-2.107
Se2	-2	-2.028
Se3	-2	-2.089
Se4	-2	-2.109

Table 5. Calculated linear and nonlinear optical coefficients of $KHg_4Ga_5Se_{12}$ and real-space atom-cutting analysis.

	d_{11} (pm/V)	d_{15} (pm/V)	d_{22} (pm/V)	d_{33} (pm/V)
$KHg_4Ga_5Se_{12}$	-44.945	45.238	-42.481	-65.257
K^+	-0.486 (1.5%)	0.374 (1.8%)	-0.339 (1.9%)	-0.898 (1.4%)
$(Hg/Ga)Se_4$	-32.763 (98.5%)	19.931 (98.2%)	-17.595 (98.1%)	-63.938 (98.6%)

For Table of Contents Only